

23.8 GHz Acoustic Filter in Periodically Poled Piezoelectric Film Lithium Niobate with 1.52 dB IL and 19.4% FBW

Sinwoo Cho, Omar Barrera, Jack Kramer, Vakhtang Chulukhadze, Tzu-Hsuan Hsu, Joshua Campbell, Ian Anderson, *Graduate Student Member, IEEE*, and Ruochen Lu., *Member, IEEE*

Abstract—This paper reports the first piezoelectric acoustic filter in periodically poled piezoelectric film (P3F) lithium niobate (LiNbO_3) at 23.8 GHz with low insertion loss (IL) of 1.52 dB and 3-dB fractional bandwidth (FBW) of 19.4%. The filter features a compact footprint of 0.64 mm^2 . The third-order ladder filter is implemented with electrically coupled resonators in 150 nm bi-layer P3F 128° rotated Y-cut LiNbO_3 thin film, operating in second-order symmetric (S2) Lamb mode. The record-breaking performance is enabled by the P3F LiNbO_3 platform, where piezoelectric thin films of alternating orientations are transferred subsequently, facilitating efficient higher-order Lamb mode operation with simultaneously high quality factor (Q) and coupling coefficient (k^2) at millimeter-wave (mmWave). Also, the multi-layer P3F stack promises smaller footprints and better nonlinearity than single-layer counterparts, thanks to the higher capacitance density and lower thermal resistance. Upon further development, the reported P3F LiNbO_3 platform is promising for compact filters at mmWave.

Index Terms—Acoustic filters, lithium niobate, millimeter-wave, periodically poled piezoelectric film (P3F), piezoelectric devices, thin-film devices.

I. INTRODUCTION

The constant pursuit of faster data rates is pushing mobile networks into millimeter-wave (mmWave) frequency bands for wider bandwidth in 5G and beyond wireless systems [1]–[3]. One key research area is compact frequency (RF) front-end components at mmWave [3]. Piezoelectric acoustic devices at RF, where electromagnetic (EM) signals are converted into and processed as mechanical vibrations [4], are good candidates, thanks to the five-order-of-magnitude shorter wavelengths of acoustic waves than EM ones [5]–[7], enabling resonators [8]–[11] and waveguiding structures [12]–[15] with smaller footprints. Because of such advantage, sub-6 GHz front-end filtering has dominantly adopted acoustics, e.g., surface acoustic wave (SAW) devices in lithium niobate (LiNbO_3), lithium tantalate (LiTaO_3), and thin-film bulk acoustic resonators (FBARs) in aluminum nitride or scandium aluminum nitride (AlN/ScAlN) [16]–[23]. It would be ideal to further leverage acoustics for mmWave RF front ends.

Manuscript received X February 2024; revised XX February 2024; accepted XX February 2024. This work was supported by DARPA COmpact Front-end Filters at the ElEment-level (COFFEE). S. Cho, O. Barrera, J. Kramer, V. Chulukhadze, J. Campbell, I. Anderson, and R. Lu are with The University of Texas at Austin, Austin, TX, USA (email: sinwoocho@utexas.edu). T.-H. Hsu, is with National Tsing Hua University, Hsinchu, Taiwan; he is currently a visiting student at The University of Texas at Austin, TX, USA. This article was presented at the IEEE MTT-S International Microwave Symposium (IMS 2024), Washington, DC, USA, June 16–21, 2024.

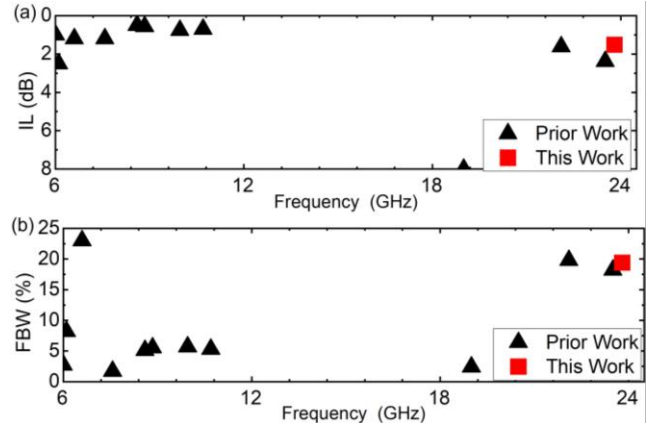


Fig. 1 Survey of (a) IL and (b) FBW in acoustic filters above 6 GHz.

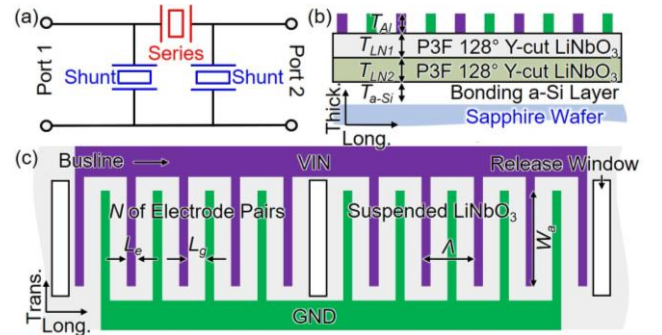


Fig. 2 (a) Filter circuit, and resonator (b) side and (c) top schematics.

However, it is unclear whether it is feasible to frequency scale application-worthy acoustic filters into mmWave. In conventional platforms, the insertion loss (IL) [Fig. 1(a)] and fractional bandwidth (FBW) [Fig. 1(b)] dramatically degrade beyond 6 GHz [21], [22], [24]–[32]. Scaling conventional acoustic devices has been limited by fabrication challenges from either very thin films or very small lateral feature sizes [33], [34]. Thin piezoelectric films tend to suffer from worse crystalline quality, while narrow electrodes introduce too much resistive loss. New platforms are required.

Recently, first-order antisymmetric mode (A1) resonators in sub-100 nm LiNbO_3 on sapphire substrate with intermediate amorphous silicon (a-Si) are demonstrated as low-loss and wideband mmWave platforms [35], [36]. Innovative design and advanced thin-film transfer collectively enable filters at 20 GHz in the state-of-the-art (SoA) (Fig. 1). Despite the great performance, the thin-film filters inherit a few issues. First, the

> REPLACE THIS LINE WITH YOUR MANUSCRIPT ID NUMBER (DOUBLE-CLICK HERE TO EDIT) <

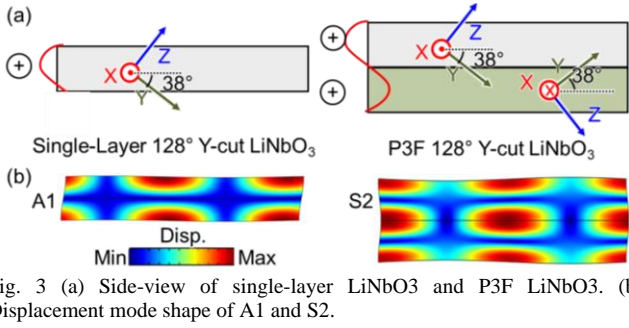


Fig. 3 (a) Side-view of single-layer LiNbO₃ and P3F LiNbO₃. (b) Displacement mode shape of A1 and S2.

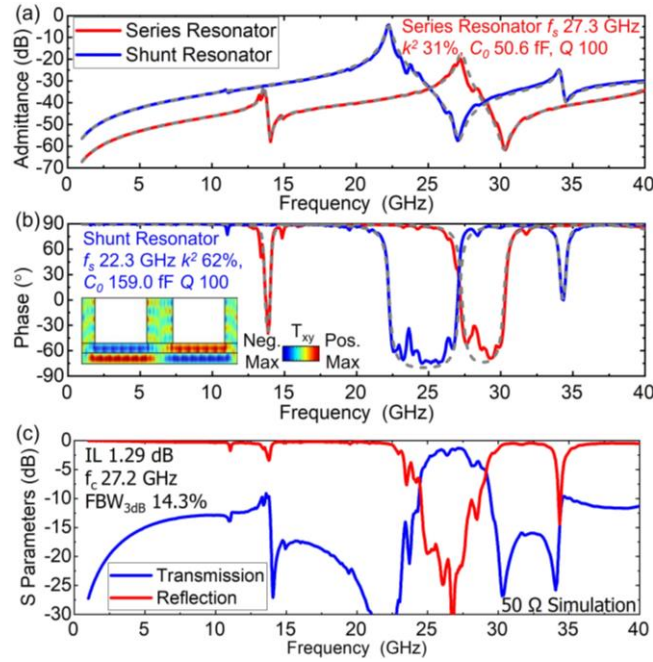


Fig. 4 Simulated admittance (a) amplitude and (b) phase, inset key specifications and vibration mode shape. (c) Simulated filter response.

thermal nonlinearity is severe [37], as the thin membrane has a large thermal resistance. Second, the footprints are large, as the lateral field excited structure has low capacitance density in thin films. The long traces, no longer electrically short, introduce undesired EM effects impacting filter performance [38]. Third, the loss in resonators is still high, marked by moderate quality factor (Q), intrinsically from the surface damping caused by the large surface-to-volume ratio [39], [40].

In this work, we demonstrate the first mmWave acoustic filters using 150 nm bi-layer periodically poled piezoelectric film (P3F) LiNbO₃ (Fig. 2), achieving low IL of 1.52 dB and 3-dB FBW of 19.4%, surpassing SoA (Fig. 1). The P3F structure promises better Q , smaller footprints, and better linearity. Upon further development, the reported P3F LiNbO₃ platform is promising for compact filters at mmWave.

II. DESIGN AND SIMULATION

The third-order ladder filter consists of one series resonator and two shunt resonators [Fig. 2 (a)] [38]. The resonators comprise 350 nm thick aluminum (Al) interdigital transducers (IDT) on the top of 150 nm thick bi-layer 128° Y-cut LiNbO₃ thin-film, suspended over a sapphire substrate with 1 μ m thick a-Si bonding and sacrificial layer [Fig. 2 (b)]. It is also reported that the a-Si layer helps preserve the quality of the transferred

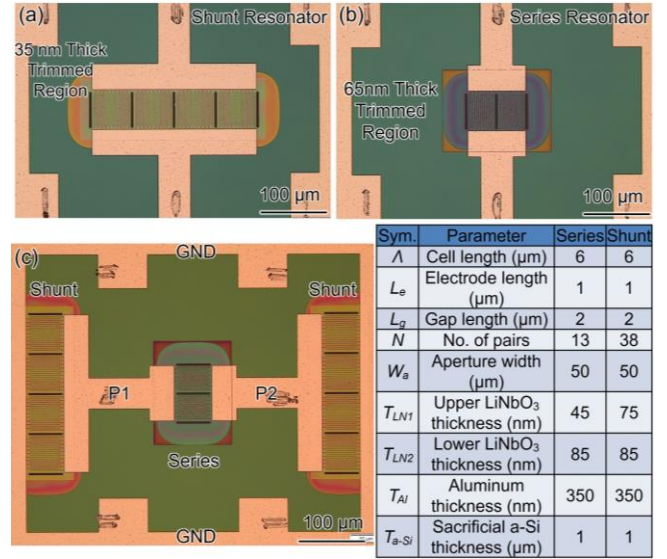


Fig. 5 Microscopic images of fabricated (a) shunt resonator, (b) series resonator, and (c) filter. Key dimensions are listed in the table.

thin-film [41]. The alternating lateral electrical fields between IDTs excite the second-order symmetric (S2) mode [Fig. 3 (b)], via the piezoelectric coefficient e_{15} in 128° Y-cut LiNbO₃. The thick electrodes on the top reduce the resistive loss and thermal resistance, while not mechanically loading the resonance as it is in the stress nodes [41]. The devices are fully anchored for higher structural strength during the release. A list of key design parameters is labeled in Fig. 2 (c) and listed in Fig. 5.

The key innovation of the work is the successful usage of the P3F LiNbO₃ stack for filters [Fig. 3 (a)], where piezoelectric thin films with opposite orientations, rotated about the axis defined by the intersection of the plane joining the two layers, are placed on top of each other, enabling higher-order mode operation in thicker films without losing electromechanical coupling (k^2) [11], [20], [42]–[45]. Specifically, the thickness of each layer matches the half wavelength in the higher-order thickness modes [Fig. 3 (a)]. Thus, piezoelectrically generated charges build up and can be effectively picked up by a single transducer on the top of the P3F stack. The P3F LiNbO₃ platform has shown promising experimental results for high-frequency operations up to 50 GHz [11], but so far, it has not been demonstrated as filters. This work aims to demonstrate the prototype. More specifically, we are using bi-layer P3F LiNbO₃ operating in S2 mode [Fig. 3 (b)], which can be intuitively thought of as bonding two A1 mode resonators in single-layer LiNbO₃ toward a thicker film, while achieving the advantages of higher Q , smaller footprint, and lower thermal resistance.

COMSOL finite element analysis (FEA) simulated S2 resonator admittance is plotted in Fig. 4 (a)-(b), showing a high k^2 of 62% for the shunt resonator at 22.3 GHz and k^2 of 31% for the series resonator at 27.3 GHz. This is obtained via a modified Butterworth-Van Dyke (MBVD) fitting with multiple motional branches [Fig. 6 (c)] [46]. Series inductor L_s and resistors R_s are ignored for FEA, as the EM effects are not coupled in COMSOL. The series and shunt resonators are designed with different film thicknesses (more specifically, 45 nm on top, 85 nm on bottom for series, and 75 nm on top, 85 nm on bottom

> REPLACE THIS LINE WITH YOUR MANUSCRIPT ID NUMBER (DOUBLE-CLICK HERE TO EDIT) <

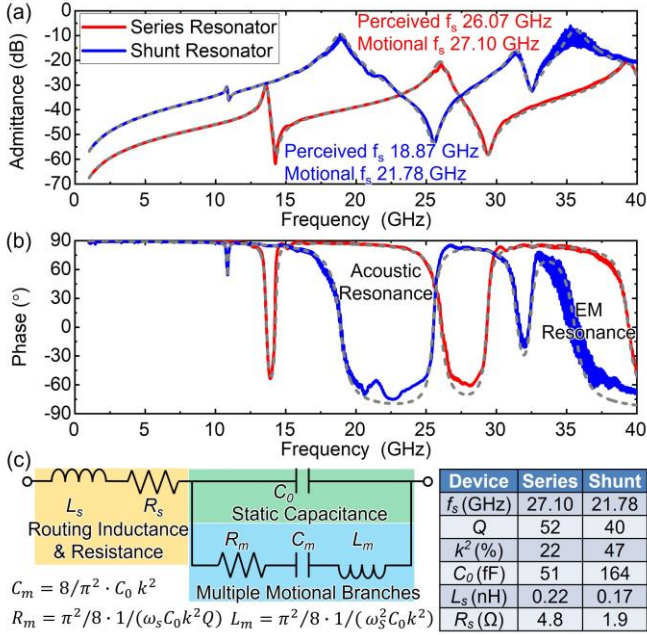


Fig. 6 Measured wideband admittance response in (a) amplitude and (b) phase. (c) Modified mmWave MBVD model and extracted key resonator specifications.

for shunt) to achieve the necessary shift in resonance (f_s) [47]. The static capacitance C_0 is chosen to match the impedance of the filter to 50Ω while providing 10 dB out-of-band (OoB) rejection. The resonator Q is assumed to be 100 conservatively which is lower than the previous LiNbO₃ P3F [44]. The simulated filter [Fig. 4 (c)] shows an IL of 1.29 dB, a center frequency (f_c) of 27.2 GHz, a 3-dB FBW of 14.3%, and an OoB of 10.1 dB. The low-loss and wideband response promise mmWave compact filter platform using P3F LiNbO₃.

III. FABRICATION AND MEASUREMENT

The stack for this work is provided by NGK Insulators Ltd. The process starts by patterning the resonator regions, then trimming the LiNbO₃ thickness of the active regions to the desired values using ion beam-assisted argon gas cluster trimming, which is reported to maintain surface roughness and high crystallinity through material analysis [48]. Next, the top electrodes are patterned with 350 nm evaporated Al IDTs. Additionally, the probing pad and routing regions are thickened up by another 350 nm evaporated Al to lower the resistive loss. Afterward, release windows are defined and etched using the ion beam. The resonator bank is divided into multiple resonators for easier release of the filters. Finally, metal electrodes are patterned, and the resonators are released through xenon difluoride (XeF₂) Si etch.

Optical images of the fabricated stand-alone shunt and series resonators and the filter are displayed in Fig. 5 (a), (b), and (c). The key dimensions are listed in Fig. 5. The filter has a small footprint of 0.85 mm by 0.75 mm.

The resonators and the filter are first measured using a Keysight vector network analyzer (VNA) in the air at a -15 dBm power level. The admittance response in amplitude and phase of the resonators are plotted in Fig. 6 (a) and (b), fitted with the mmWave MBVD circuit model [41] in Fig. 6 (c).

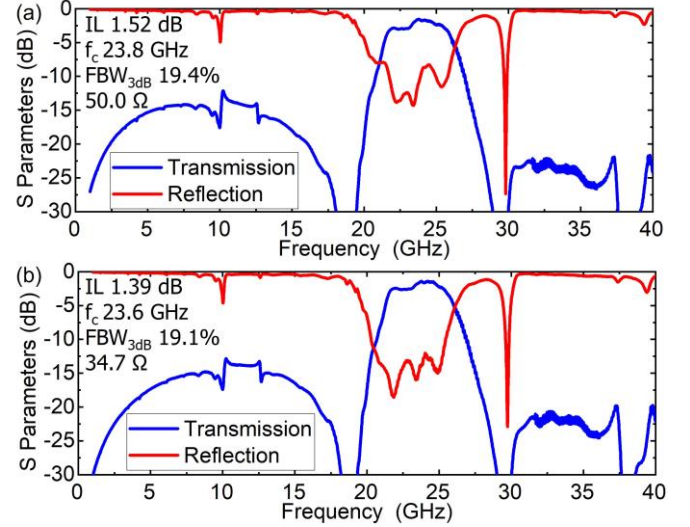


Fig. 7 Measured filter wideband transmission and reflection with (a) 50Ω and (b) matched to 34.7Ω port impedance.

A higher frequency resonance of electromagnetic (EM) nature occurs due to the self-resonance of the reactive parasitic embedded in the resonator routing. L_s and routing resistance R_s are fitted based on EM resonances. Another effect is that the perceived resonances are now at 26.07 GHz for the series and 18.87 GHz for the shunt, which deviate from the mechanical resonances represented by the motional elements L_m , C_m , and R_m . The measurements show Q around 40 and a high k^2 of around 47% (Fig. 6 inset table). k^2 is obtained via MBVD fitting, which is smaller than the perceived k^2 calculated from f_s and f_p , due to the existence of L_s [41]. Q is defined as the anti-resonance due to the inclusion of R_s and L_s .

The measured filter response under 50Ω is shown in Fig. 7 (a). The 23.8 GHz filter exhibits a low IL of 1.52 dB IL, a wide 3-dB FBW of 19.4%, a 30 dB Shape Factor of 2.08, and an OoB rejection of 12.1 dB, matching device simulation. The measured filter response under resistance matched 34.7Ω in Fig. 7 (b) shows a passband centered at 23.6 GHz with IL of 1.39 dB, broad 3-dB FBW of 19.1%, OoB rejection of 12.8 dB and 30 dB Shape Factor of 2.16. Compared with SoA low-loss acoustic filters (Fig. 1), this work shows significant frequency scaling and FBW enhancement. The reduced OoB performance is a drawback of using a low order filter with only three resonators and will be improved in future works.

IV. CONCLUSION

In this work, we demonstrate the first mmWave acoustic filters using 150 nm bi-layer P3F LiNbO₃, achieving low IL of 1.52 dB and 3-dB FBW of 19.4%, surpassing SoA. The P3F structure promises better Q , smaller footprints, and better linearity. Upon further development, the reported P3F LiNbO₃ platform is promising for compact filters at mmWave.

ACKNOWLEDGMENT

The authors would like to thank the funding support from the DARPA COFFEE program and Dr. Ben Griffin and Dr. Todd Bauer for helpful discussions.

REFERENCES

- [1] R. Aigner *et al.*, “BAW Filters for 5G Bands,” in *Technical Digest - International Electron Devices Meeting, IEDM*, 2018.
- [2] M. Matthaiou *et al.*, “The road to 6G: Ten physical layer challenges for communications engineers,” *IEEE Communications Magazine*, vol. 59, no. 1, 2021.
- [3] A. Hagelauer *et al.*, “From Microwave Acoustic Filters to Millimeter-Wave Operation and New Applications,” *IEEE Journal of Microwaves*, vol. 3, no. 1, 2022.
- [4] G. Piazza, “Piezoelectric Resonant MEMS,” in *Resonant MEMS: Principles, Modeling, Implementation, and Applications*, 2015.
- [5] R. Lu and S. Gong, “RF acoustic microsystems based on suspended lithium niobate thin films: Advances and outlook,” *Journal of Micromechanics and Microengineering*, vol. 31, no. 11, 2021.
- [6] S. Gong *et al.*, “Microwave Acoustic Devices: Recent Advances and Outlook,” *IEEE Journal of Microwaves*, vol. 1, no. 2, 2021.
- [7] R. Ruby, “A snapshot in time: The future in filters for cell phones,” *IEEE Microw Mag*, vol. 16, no. 7, 2015.
- [8] Z. Schaffer *et al.*, “A Solidly Mounted 55 GHz Overmoded Bulk Acoustic Resonator,” in *2023 IEEE International Ultrasonics Symposium (IUS)*, 2023.
- [9] G. Giribaldi *et al.*, “High-Crystallinity 30% ScAlN Enabling High Figure of Merit X-Band Microacoustic Resonators for Mid-Band 6G,” in *IEEE MEMS*, 2023.
- [10] S. Cho *et al.*, “Millimeter Wave Thin-Film Bulk Acoustic Resonator in Sputtered Scandium Aluminum Nitride,” *Journal of Microelectromechanical Systems*, vol. 32, no. 6, pp. 529–532, 2023.
- [11] R. Vetry *et al.*, “A Manufacturable AlScN Periodically Polarized Piezoelectric Film Bulk Acoustic Wave Resonator (AlScN P3F BAW) Operating in Overtone Mode at X and Ku Band,” in *IEEE International Microwave Symposium - IMS*, 2023, pp. 891–894.
- [12] S. Cho *et al.*, “Acoustic Delay Lines in Thin-Film Lithium Niobate on Silicon Carbide,” in *2022 IEEE/MTT-S International Microwave Symposium - IMS*, 2022, pp. 809–812.
- [13] S. Cho *et al.*, “Analysis of 5-10 GHz Higher-Order Lamb Acoustic Waves in Thin-Film Scandium Aluminum Nitride,” in *IFCS-EFTF 2023, Proceedings*, Toyama, Japan: IEEE, 2023.
- [14] G. Giribaldi *et al.*, “Low Propagation Loss X-Band Impedance Matched Lamb Mode Delay Lines in 30% Scandium Aluminum Nitride,” in *2023 IEEE International Ultrasonics Symposium*, 2023.
- [15] J. Kramer *et al.*, “Extracting Acoustic Loss of High-Order Lamb Modes at Millimeter-Wave Using Acoustic Delay Lines,” in *2023 IEEE/MTT-S International Microwave Symposium - IMS 2023*, 2023, pp. 903–906.
- [16] G. Esteves *et al.*, “Al_{0.68}Sc_{0.32}N Lamb wave resonators with electromechanical coupling coefficients near 10.28%,” *Appl Phys Lett*, vol. 118, no. 17, p. 171902, Apr. 2021.
- [17] L. Colombo *et al.*, “Investigation of 20% scandium-doped aluminum nitride films for MEMS laterally vibrating resonators,” in *2017 IEEE International Ultrasonics Symposium (IUS)*, 2017.
- [18] M. D. Henry *et al.*, “AlN and ScAlN Contour Mode Resonators for RF Filters,” *ECS Trans*, vol. 77, no. 6, p. 23, Apr. 2017.
- [19] R. H. Olsson *et al.*, “A high electromechanical coupling coefficient SH₀ Lamb wave lithium niobate micromechanical resonator and a method for fabrication,” *Sens Actuators A Phys*, vol. 209, pp. 183–190, 2014.
- [20] J. Kramer *et al.*, “Trilayer Periodically Poled Piezoelectric Film Lithium Niobate Resonator,” in *IEEE International Ultrasonics Symposium (IUS)*, 2023.
- [21] Y. Yang *et al.*, “4.5 GHz Lithium Niobate MEMS Filters with 10% Fractional Bandwidth for 5G Front-Ends,” *Journal of Microelectromechanical Systems*, vol. 28, no. 4, 2019.
- [22] P. J. Turner *et al.*, “5 GHz band n79 wideband microacoustic filter using thin lithium niobate membrane,” *Electron Lett*, vol. 55, no. 17, 2019.
- [23] S. Cho *et al.*, “Millimeter Wave Thin-Film Bulk Acoustic Resonator in Sputtered Scandium Aluminum Nitride Using Platinum Electrodes,” *IEEE International Conference on Micro Electro Mechanical Systems (MEMS)*, 2024.
- [24] L. Zhang *et al.*, “High-Performance Acoustic Wave Devices on LiTaO₃/SiC Hetero-Substrates,” *IEEE Trans Microw Theory Tech*, vol. 71, no. 10, pp. 4182–4192, 2023.
- [25] R. Su *et al.*, “Scaling Surface Acoustic Wave Filters on LNOI platform for 5G communication,” in *Technical Digest - International Electron Devices Meeting, IEDM*, 2022.
- [26] D. Kim *et al.*, “Wideband 6 GHz RF Filters for Wi-Fi 6E Using a Unique BAW Process and Highly Sc-doped AlN Thin Film,” in *IEEE MTT-S International Microwave Symposium Digest*, 2021.
- [27] R. Vetry *et al.*, “High Power, Wideband Single Crystal XBAW Technology for sub-6 GHz Micro RF Filter Applications,” in *IEEE International Ultrasonics Symposium, IUS*, 2018.
- [28] T. Kimura *et al.*, “Comparative Study of Acoustic Wave Devices Using Thin Piezoelectric Plates in the 3-5-GHz Range,” in *IEEE IEEE Trans Microw Theory Tech*, 2019, pp. 915–921.
- [29] Y. Yang *et al.*, “X-Band Miniature Filters Using Lithium Niobate Acoustic Resonators and Bandwidth Widening Technique,” *IEEE Trans Microw Theory Tech*, vol. 69, no. 3, 2021.
- [30] L. Gao *et al.*, “Wideband Hybrid Monolithic Lithium Niobate Acoustic Filter in the K-Band,” *IEEE Trans Ultrason Ferroelectr Freq Control*, vol. 68, no. 4, 2021.
- [31] M. Aljoumayly *et al.*, “5G BAW Technology: Challenges and Solutions,” in *IEEE Wireless and Microwave Technology Conference*, 2022.
- [32] G. Giribaldi *et al.*, “Compact and wideband nanoacoustic pass-band filters for future 5G and 6G cellular radios,” *Nat Commun*, vol. 15, no. 1, p. 304, 2024.
- [33] Z. Schaffer *et al.*, “33 GHz Overmoded Bulk Acoustic Resonator,” *IEEE Microwave and Wireless Components Letters*, vol. 32, no. 6, pp. 656–659, 2022.
- [34] M. Rinaldi *et al.*, “Super-high-frequency two-port AlN contour-mode resonators for RF applications,” *IEEE Trans Ultrason Ferroelectr Freq Control*, vol. 57, no. 1, pp. 38–45, 2010.
- [35] O. Barrera *et al.*, “Transferred Thin Film Lithium Niobate as Millimeter Wave Acoustic Filter Platforms,” in *IEEE International Conference on Micro Electro Mechanical Systems (MEMS)*, 2024.
- [36] O. Barrera *et al.*, “Thin-Film Lithium Niobate Acoustic Filter at 23.5 GHz With 2.38 dB IL and 18.2% FBW,” *Journal of Microelectromechanical Systems*, vol. 32, no. 6, pp. 622–625, 2023.
- [37] J. Segovia-Fernandez and G. Piazza, “Thermal nonlinearities in contour mode AlN resonators,” *Journal of Microelectromechanical Systems*, vol. 22, no. 4, 2013.
- [38] D. M. Pozar, *Microwave engineering / David M. Pozar*. 2017.
- [39] R. Lu, Y. Yang, and S. Gong, “Acoustic Loss of GHz Higher-Order Lamb Waves in Thin-Film Lithium Niobate: A Comparative Study,” *Journal of Microelectromechanical Systems*, vol. 30, no. 6, 2021.
- [40] M. Rinaldi, C. Zuniga, and G. Piazza, “5-10 GHz ALN contour-mode nanoelectromechanical resonators,” in *Proceedings of the IEEE International Conference on Micro Electro Mechanical Systems (MEMS)*, 2009.
- [41] J. Kramer *et al.*, “57 GHz Acoustic Resonator with k₂ of 7.3 % and Q of 56 in Thin-Film Lithium Niobate,” in *IEEE International Electron Devices Meeting (IEDM)*, 2022, pp. 16.4.1-16.4.4.
- [42] R. Lu *et al.*, “Enabling Higher Order Lamb Wave Acoustic Devices with Complementarily Oriented Piezoelectric Thin Films,” *Journal of Microelectromechanical Systems*, vol. 29, no. 5, 2020.
- [43] S. Nam *et al.*, “A mm-Wave Trilayer AlN/ScAlN/AlN Higher Order Mode FBAR,” *IEEE Microwave and Wireless Technology Letters*, vol. 33, no. 6, 2023.
- [44] J. Kramer *et al.*, “Thin-Film Lithium Niobate Acoustic Resonator with High Q of 237 and k₂ of 5.1% at 50.74 GHz,” in *IFCS-EFTF 2023, Proceedings*, 2023, pp. 1–4.
- [45] Izhar *et al.*, “A K-Band Bulk Acoustic Wave Resonator Using Periodically Poled Al_{0.72}Sc_{0.28}N,” *IEEE Electron Device Letters*, 2023.
- [46] R. Lu *et al.*, “Accurate extraction of large electromechanical coupling in piezoelectric MEMS resonators,” *Journal of Microelectromechanical Systems*, vol. 28, no. 2, 2019.
- [47] E. Guerrero *et al.*, “A Synthesis Approach to Acoustic Wave Ladder Filters and Duplexers Starting With Shunt Resonator,” *IEEE Trans Microw Theory Tech*, vol. 69, no. 1, pp. 629–638, 2021.
- [48] V. Chulukhadze *et al.*, “Frequency Scaling Millimeter Wave Acoustic Devices in Thin Film Lithium Niobate,” in *IEEE International Frequency Control Symposium (IFCS)*, 2023.